


---

This is the **submitted version** of the journal article:

Norjmaa, Gantulga; Maréchal, Jean-Didier; Ujaque Pérez, Gregori. «Micro-solvation and Encapsulation Effects on Supramolecular Catalysis : CC Reductive Elimination inside [Ga<sub>4</sub>L<sub>6</sub>] 12- Metallocage». Journal of the American Chemical Society, Vol. 141, Issue 33 (August 2019), p. 13114-13123. DOI 10.1021/jacs.9b04909

---

This version is available at <https://ddd.uab.cat/record/279254>

under the terms of the  **CC BY-NC-ND** license

# Microsolvation and Encapsulation Effects on Supramolecular Catalysis: C-C Reductive Elimination inside [Ga<sub>4</sub>L<sub>6</sub>]<sup>12-</sup> Metallocage

Gantulga Norjmaa, Jean-Didier Maréchal\* and Gregori Ujaque\*

Departament de Química, Universitat Autònoma de Barcelona, 08193 Cerdanyola del Valles, Barcelona, Catalonia, Spain

**KEYWORDS:** *Supramolecular catalysis, homogeneous catalysis, host-guest complexes, metallocage, reductive elimination, density functional theory, molecular dynamics.*

## Abstract

In this study, the host effect of the supramolecular [Ga<sub>4</sub>L<sub>6</sub>]<sup>12-</sup> tetrahedral metallocage on reductive elimination of substrate by encapsulated Au(III) complexes is investigated by means of computational methods. The behavior of the reactants in solution and within the metallocage is initially evaluated by means of classical molecular dynamics simulations. These results guided the selection of proper computational models to describe the reaction in solution and inside the metallocage at DFT level. The calculated Gibbs energy barriers are in very good agreement with experiment both in solution and inside the metallocage. The analysis in solution revealed that microsolvation around the Au(III) complex increases the Gibbs energy barrier. The analysis within metallocage shows that its encapsulation favors the reaction. The process can be formally described as removing explicit microsolvation around the gold complex and encapsulating the metal complex inside the metallocage. Both processes are important for the reaction but the removal of the solvent molecules surrounding the Au(III) metal complex is fundamental for the reduction of the reaction barrier. The energy decomposition analysis of the barrier among strain, interaction and thermal terms shows that strain term is very low whereas the contribution of thermal (entropic) effects is moderate. Interestingly, the key term responsible for reducing the Gibbs energy barrier is the interaction. This term can be mainly associated to electrostatic interactions in agreement with previous examples in the literature.

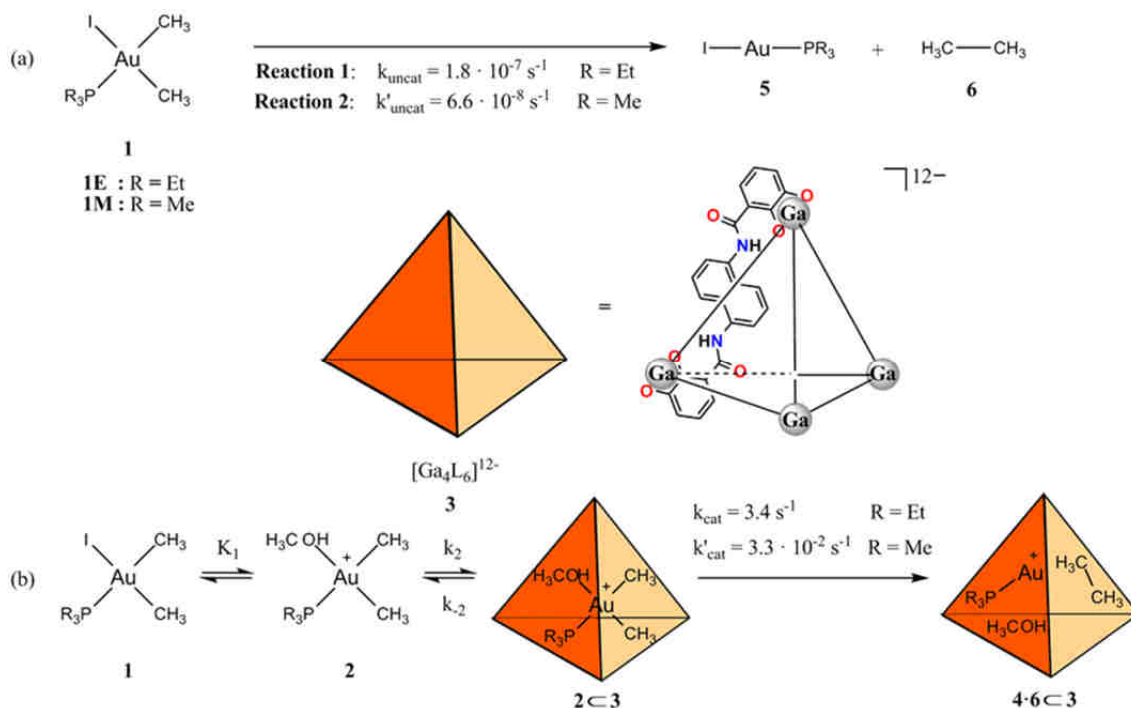
## 1. INTRODUCTION

Supramolecular catalysis is a discipline that brings together the fields of catalysis and supramolecular chemistry.<sup>1</sup> The design of molecular compounds offering cavities is of great interest since they can become enzyme-like catalysts for chemical transformations. They were initially inspired in biological processes although their design has significantly evolved, and many new man-made microenvironments have been developed.

The molecular compounds able to mediate or catalyze chemical reactions are also named molecular flasks.<sup>2,3</sup> The first example of a molecular flask was published by Rebek based on a purely organic cage assembled via hydrogen-bonding interactions.<sup>4-6</sup> Synthetic cages based on metal-organic coordination structures, named metallocages represent a recognized development in host design.<sup>7-16</sup> They are very interesting due to the large versatility generated by including metals in their structure. In this sense, several metallocages have been designed as supramolecular catalysts<sup>17-21</sup> including Raymond's<sup>22</sup> Ga<sub>4</sub>L<sub>6</sub>, Fujita's<sup>23</sup> Pd<sub>6</sub>L<sub>4</sub> or Nitschke's<sup>24</sup> Fe<sub>4</sub>L<sub>6</sub>, among others.<sup>25-27</sup>

The tetrahedron host K<sub>12</sub>[Ga<sub>4</sub>L<sub>6</sub>] developed by Raymond and coworkers has been applied to catalyze a set of reactions including the hydrolysis of orthoformates,<sup>28</sup> Nazarov cyclization,<sup>29</sup> hydroalkylation,<sup>30</sup> allyl alcohol isomerization,<sup>31</sup> aza-Cope rearrangement,<sup>32</sup> etc.<sup>33,34</sup> The metallocage catalyzes the reductive elimination for several high-valent transition metal based on Au(III) and Pt(IV) complexes.<sup>35,36</sup> In this work we are interested in the alkyl-alkyl reductive elimination from a Au(III) complex. The reaction is dramatically accelerated when performed inside the [Ga<sub>4</sub>L<sub>6</sub>]<sup>12-</sup> metallocage, becoming the highest accelerated reaction observed to up to date for any synthetic supramolecular catalyst.<sup>35</sup> This reaction has been deeply investigated by Bergman, Raymond and Toste, thus, there is a large amount of experimental information available.

A schematic representation of the process involving gold species is presented in Scheme 1. According to the kinetic experiments the reaction is consistent with a Michaelis-Menten-type mechanism; it is described by a preequilibrium process of halide dissociation previous to the encapsulation of the emerging cationic Au(III)-complex by the supramolecular [Ga<sub>4</sub>L<sub>6</sub>]<sup>12-</sup> metallocage, **3**. For the case of complex **1E**, [(Et<sub>3</sub>P)Au(I)(CH<sub>3</sub>)<sub>2</sub>], they observed an outstanding value for the acceleration rate,  $k_{\text{cat}}/k_{\text{uncat}}$ , of  $1.9 \times 10^7$  when comparing the processes in MeOH solvent in the presence/absence of metallocage **3**. The rate acceleration,  $k_{\text{cat}}/k_{\text{uncat}}$ , for complex **1M**, with a Me<sub>3</sub>P phosphine in the Au(III) coordination sphere is  $5.0 \times 10^5$ . For the case of Ph<sub>3</sub>P phosphine as ligand no acceleration is observed indicating size exclusion of the Au(III)-complex from the cavity of metallocage **3**.



**Scheme 1.** Schematic representation of the reductive elimination from  $[(\text{R}_3\text{P})\text{Au}(\text{I})(\text{CH}_3)_2]$  complexes, **1E** and **1M**: (a) in MeOH solution and (b) and inside  $[\text{Ga}_4\text{L}_6]^{12-}$  metallocage **3**.\*

Theoretical analysis is nowadays indispensable to acquire a deeper understanding at a molecular level of catalytic processes.<sup>37,38</sup> However, few theoretical studies of the rate acceleration by supramolecular hosts have been reported. Some examples are cycloaddition inside cucurbit[6]uril<sup>39,40</sup> and inside Rebek's capsule,<sup>41</sup> Diels-Alder reactions inside  $\beta$ -cyclodextrin ( $\beta$ -CD)<sup>42</sup> and in Rebek's "softball",<sup>43</sup> among others.<sup>44–50</sup> For metallocages, and more particular for the case of the Raymond  $[\text{Ga}_4\text{L}_6]^{12-}$  metallocage the orthoformate hydrolysis<sup>51</sup> and aza-Cope rearrangement<sup>52</sup> have been theoretically investigated and in a recent work by Vaissier-Welborn and Head-Gordon<sup>53</sup> the effect of the overall charge of the  $[\text{M}_4\text{L}_6]$  metallocage on the C-C reductive elimination process (by comparing  $[\text{Ga}_4\text{L}_6]^{12-}$  with  $[\text{Si}_4\text{L}_6]^{8-}$ , respectively) was also computationally investigated. Most of these works concluded that the electrostatic environment is essential for increasing the reaction rate.

The aim of the present work is to investigate the origin of the outstanding rate acceleration between encapsulated and non-encapsulated complexes by comparing the reaction in methanol and inside the metallocage by means of theoretical methods. In our study we also observed that the electrostatic surrounding is important, but importantly, we identified and quantified the two main factors for reducing the energy barrier: change in the microsolvation and encapsulation of the reactant. We also addressed additional questions as if the  $\text{K}^+$  counterions affect the metallocage activity, are there solvent molecules inside the cavity, how important are the entropic effects, etc. Answering these questions should help the design of new supramolecular catalysts.

## 2. COMPUTATIONAL DETAILS

All DFT calculations were performed with the B3LYP-D3 functional<sup>54</sup> as implemented in the Gaussian 09 software package.<sup>55</sup> Geometry optimizations were performed with the 6-31G(d) basis set for the main group elements and the scalar relativistic Stuttgart–Dresden (SDD) pseudopotential complemented with a set of d and f polarization functions for the gallium and gold atoms, respectively.<sup>56,57</sup> The structures of the reactants, transition states, and products were optimized in methanol solvent using the SMD polarizable continuum model<sup>58</sup> and three-body DFT-D3 dispersion corrections<sup>59</sup> were added separately. Additional test calculations using PCM<sup>60,61</sup> were also performed showing a similar trend (see Sup. Inf. Table S2). The largest model used in DFT calculations contains 328 atoms (3401 basis functions) with average calculations of around 300 atoms. The quasi-rigid-rotor-harmonic-oscillator (quasi-RRHO) approach was used for thermal contributions to the Gibbs energies.<sup>62</sup> The standard state corrections<sup>63</sup> to the Gibbs energies are calculated with the correction term  $[RT \ln(1/24.46 \text{ L/mol} \times 1 \text{ mol/L})]$ ; thus, 1.9 kcal/mol was added to each of the compounds except methanol for which the correction term  $RT \ln(1/24.46 \text{ L/mol} \times 24.75 \text{ mol/L})$  is 3.8 kcal/mol.

For the reaction in solution DLPNO-CCSD(T) calculations<sup>64</sup> were performed with ORCA 4.0<sup>65</sup> to compare with B3LYP-D3 results. We compared DLPNO-CCSD(T) and B3LYP-D3 energy barriers of the model reaction in vacuum and with SMD solvation in MeOH. The difference between the calculated energy barriers at these two levels of theory is only around 1.0 kcal/mol (see Sup. Inf. Table S3).

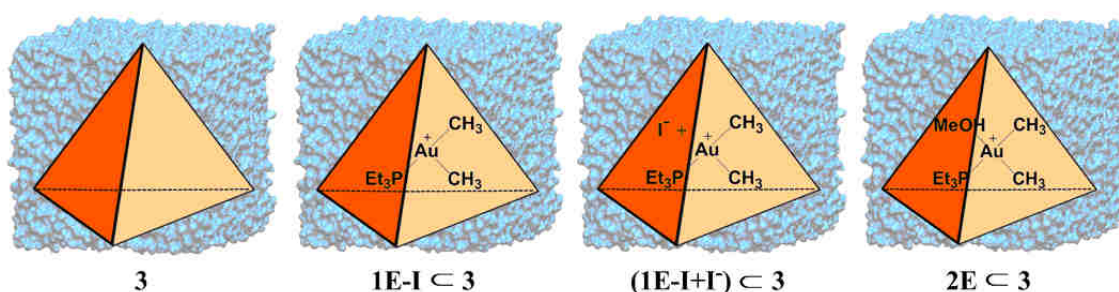
To find out the number of solvent molecules inside the cavity of the metallocage classical Molecular Dynamics (MD) simulations were performed with more than 3500 explicit methanol solvents (MEOHBOX) and the number of K<sup>+</sup> counterions necessary to keep the solution neutral. All MD simulations were performed using Amber 16 suite of programs<sup>66</sup> with a general AMBER force field.<sup>67</sup> A cubic periodic box (68 Å length of the edge), which is close to the experimental concentration of the metallocage) under the NPT conditions (P = 1 bar, T = 298.15K). Productive simulation runs of 400 ns were considered after an equilibration period of 60 ps. The MD simulation of **1E-I** in solution was performed with a periodic box of 50 Å x 50 Å x 50 Å including around 1660 methanol solvent molecules. The MCPB.py program<sup>68</sup> was used to generate parameters and the antechamber<sup>69</sup> was employed for the RESP charge<sup>70</sup> derivation. The cavity volumes were obtained using the CAVER Analyst 1.0 software tool employing the default probe radii.<sup>71</sup> To obtain an initial geometry for the DFT calculation of the neutral system including K<sup>+</sup> ions surrounding the metallocage we performed a MD simulation of 2 ns under solvent-free conditions. The last snapshot was the taken as starting point for DFT geometry optimizations.

### 3. RESULTS AND DISCUSSION

The description of the results and discussion is divided in three main subsections. The first one is devoted to the describe the Molecular Dynamic simulations of the Au(III) intermediates inside the supramolecular metallocage, **3**, on a periodic box of MeOH solvent. The following subsection describes the quantum mechanical results on the reductive elimination process of the Au(III)-complex inside the  $M_4L_6$  supramolecular cage. The next subsection describes the results for the reductive elimination reaction in MeOH solution. Finally, there is a discussion on the origin of the catalytic effect of the supramolecular metallocage compared to the reaction in solution.

#### 3.1. Molecular Dynamics Simulations

In this section the behavior of the  $[Ga_4L_6]^{12-}$  metallocage as well as the encapsulated intermediates that have been postulated to be involved in the process are evaluated by means of molecular dynamic simulations within a periodic box of explicit MeOH solvent molecules (Scheme 2). For analytical purposes the “empty” metallocage, **3**, was first considered. Then, two different models with the gold(III) complex inside the cavity were also simulated: one is the **2E** complex encapsulated, labelled as **2E** $\subset$ **3**, whereas the other includes the T-shaped Au(III)-complex, **1E-I**, encapsulated, labelled as **1E-I** $\subset$ **3**. Moreover, a system including the later complex, **1E-I** and an iodide ion,  $I^-$ , as separated entities both encapsulated, labelled as **(1E-I+I<sup>-</sup>)** $\subset$ **3**, was also investigated. All the simulations included the proper number of explicit  $K^+$  ions to keep neutrality of the system.



**Scheme 2.** Schematic representation of the systems studied by means of molecular dynamic simulations inside a periodic box of MeOH.

For the case of the initial “empty”  $[Ga_4L_6]^{12-}$  metallocage **3** in solution (including 12  $K^+$  to keep electroneutrality) an average range of 5-8 solvent MeOH molecules were observed to be inside the cavity during the simulation time (Figure S3). The analysis of the MD trajectories shows that there is a range of 6-9  $K^+$  ions around the cage (Figure S4), with up to two standing inside the cavity (Figure S5). Thus, the apparent charge of the metallocage counting the surrounding  $K^+$  ions in solution is in the range from -6 to -3. This is in reasonable agreement with the experimental measured charge of -4 and -3 for metallocage, **3**, with encapsulated  $Et_4N^+$  in solution.<sup>8,72</sup>

The simulation of **(1E-I+I<sup>-</sup>)C3**, shows that the iodide ion releases the cavity at the very beginning of the simulation (in less than 2 ns). This indicates that the un-coordinated iodide can rapidly release the cavity of the metallocage, in agreement with experimental<sup>35</sup> and previous theoretical calculations.<sup>53</sup> The simulation also shows that in this system one solvent MeOH molecule stands inside the cavity in close contact with the gold complex **1E-I**, Figure S10b. Such behavior is also observed in the simulation that starts with the **1E-I** complex without iodide inside the metallocage, **1E-I-C3**. These results strongly support that the “real” form of the gold complex encapsulated in the cavity is the methanol coordinated system with the iodide being already released, **2E-C3** in agreement with experiment. The simulation on this system shows that the cavity excludes further solvent molecules; only in very few configurations a second solvent molecule fits (see Sup. Inf. Figure S10c). This indicates that encapsulated intermediate **2E** can be mainly described as an “isolated” molecule inside the cavity. This result shows how illustrative are simulations to identify the number of molecules inside the cavity during the process and represents a fundamental step in selecting the chemical models to be considered to investigate the process by means of DFT calculations.

### **3.2 Reductive elimination of [L<sub>n</sub>Au(CH<sub>3</sub>)<sub>2</sub>]<sup>+</sup> inside the [Ga<sub>4</sub>L<sub>6</sub>]<sup>12-</sup> metallocage**

This section is devoted to the analysis of the reductive elimination process inside the metallocage by means of DFT calculations including continuum solvation model. MD calculations show that at the maximum two solvent molecules can be present inside the cavity. Thus, we calculated the reactants and transition states for the reductive elimination process on the [L<sub>n</sub>Au(CH<sub>3</sub>)<sub>2</sub>]<sup>+</sup> complex considering 0, 1 and 2 MeOH within the cavity. Reaction profiles for each of the systems are presented in Figure 1.

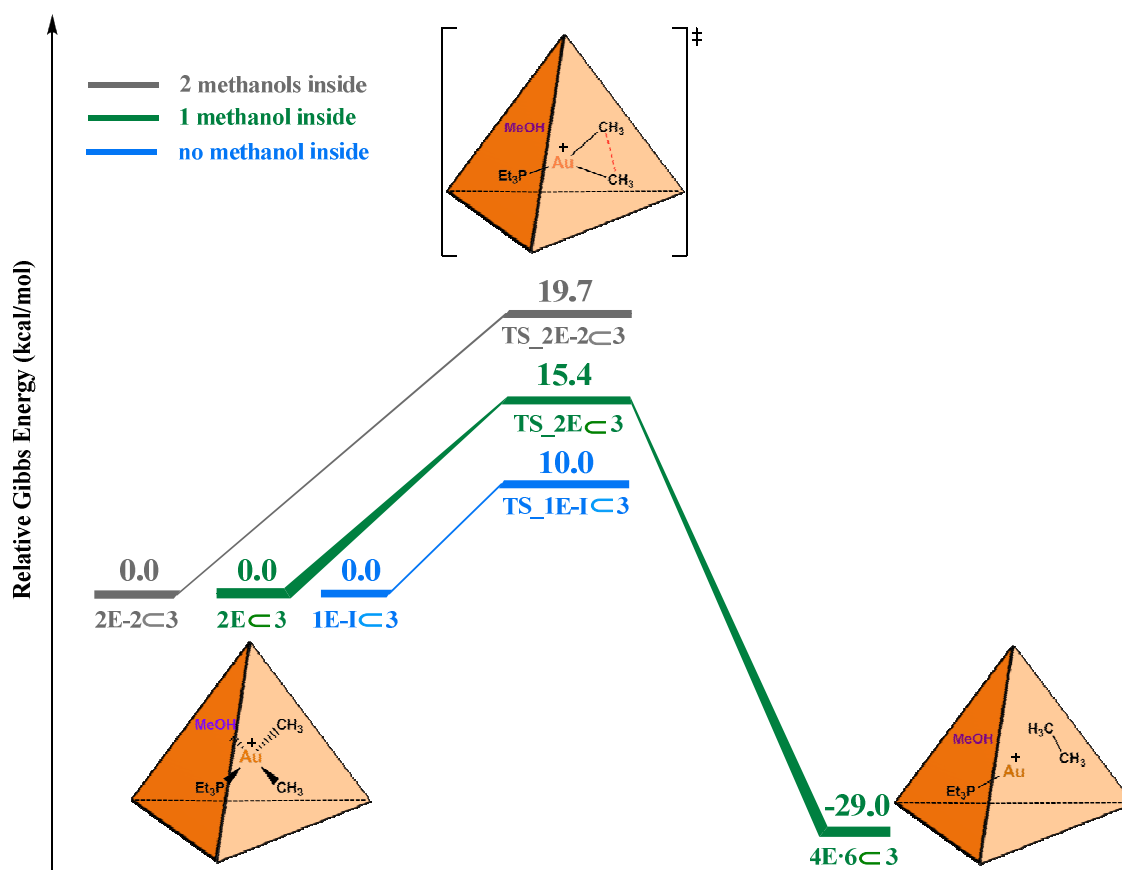


**Figure 1.** Gibbs energy profile for the reductive elimination including 0 (**1E-1C3**), 1 (**2E<C3**) and 2 (**2E-2**) MeOH solvent molecules inside the cavity.

According to the results shown in Figure 1 the reaction barrier changes significantly depending on the number of solvent molecules considered inside the cavity. For the system with no explicit MeOH solvent molecules the Gibbs energy barrier from reactant **1E-1C3** to transition state **TS\_1E-1C3** is 10.0 kcal/mol. The forming C-C bond distance is 2.182 Å. The model that has one explicit MeOH occupying a coordination site of the square planar Au(III) complex, **2E**, presents a Gibbs energy barrier of 15.4 kcal/mol. At the transition state **TS\_2E<C3**,<sup>73</sup> the distance between the two carbon atoms is 2.189 Å; the Au...O<sub>MeOH</sub> distance is 4.728 Å, indicating that the MeOH is no longer coordinated to the gold center at the transition state (Figure 2).<sup>74</sup> We also calculated the profile for the model that includes two explicit MeOH molecules (one coordinated), **2E-2C3**. The Gibbs energy barrier is 19.7 kcal/mol, with a forming C-C bond distance of 2.179 Å, and a Au...O<sub>MeOH</sub> distance of 3.299 Å in **TS\_2E-2C3**.

The Gibbs energy barrier is highly affected by the number of explicit MeOH present in the calculation. The experimental estimated value for the Gibbs energy barrier is 16.7 kcal/mol.<sup>35</sup> Looking at the three models considered, the one including a single (coordinated) MeOH molecule, **2E<C3** provides the closest energy barrier to the experimental value. Note that MD simulations also suggest that complex **2E<C3** is the most populated structure. These results show therefore that not only the system with a unique methanol molecule in the cavity is the most populated one, it appears to be



the only one that lead to relevant catalytic structures. We calculated the weighted average Gibbs energy barrier considering that these pathways can be competing. In a molecular dynamics simulations of **2Ec3**, the ratio of 0 to 1 additional MeOH inside the cavity was 391:9. The weighted averaged Gibbs energy barrier is then  $[(391 \cdot 15.4 + 9 \cdot 19.7) / 400] = 15.5$  kcal/mol, also in very good agreement with experiment.

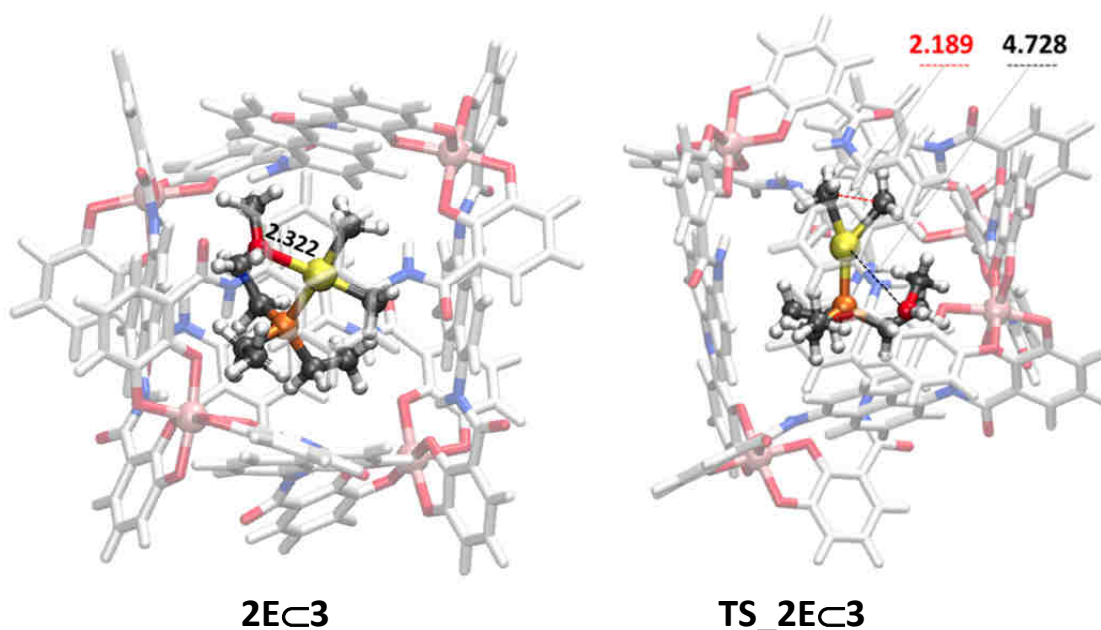


Figure 2. Optimized geometries of encapsulated reactant, **2Ec3**, and transition state, **TS\_2Ec3**. The cage is made transparent for clarity.

The effect of  $K^+$  counter ions surrounding the metallocage on the Gibbs energy barrier was also evaluated, see Table 1. During 400 ns classical MD simulation of **2Ec3**, there is an average of seven  $K^+$  ions at a lower distance of 11 Å from the center of mass of the metallocage (all of them outside the cavity; see Sup. Inf. Figure S9). This is in excellent agreement with experimentally<sup>8,72</sup> charge of -4 and -3 observed for the encapsulated  $Et_4N^+$  in **3**. Based on this observation we recalculated at DFT level the reductive elimination Gibbs energy barrier for a system including 7  $K^+$  surrounding the metallocage, (**2Ec3K7** to **TS\_2Ec3K7**; geometry shown in Figure S12). Interestingly, the Gibbs energy barrier is 15.4 kcal/mol, very similar to the metallocage without counterions.

Table 1. Calculated Gibbs energy barriers for the system **2Ec3** including a different number of  $K^+$  counterions.

Optimized geometry of TS		Number of $K^+$	Total charge	$\Delta G^\ddagger_{\text{calc}}$	$\Delta G^\ddagger_{\text{exp}}$
Name	C-C distance (Å)				
<b>TS_2Ec3</b>	2.19	0	-11	15.4	16.7
<b>TS_2Ec3K7</b>	2.16	7	-4	15.4	
<b>TS_2Ec3K11</b>	2.16	11	0	15.1	

The energy barrier for the neutral system (including 11  $K^+$  ions surrounding the metallogage) was also computed. The geometries for the reactant, **2E** $\llcorner$ **3K11**, and the transition state, **TS\_2E** $\llcorner$ **3K11**, were optimized (Figure S13). The energy barrier of this system is also very similar to the previous cases, 15.1 kcal/mol, which highlights that the number counter ions surrounding the metallogage do not significantly influence the Gibbs energy barrier of the reaction.<sup>75</sup> A deeper analysis on this fact is presented in section 11 on Sup. Inf. However, to check how the local environment inside the cavity influences the reaction we need to compare it with the reaction in MeOH solution.

### 3.3 Reductive elimination of $[L_nAu(CH_3)_2]^+$ in MeOH solution

This section analyzes the reductive elimination process for the  $[L_nAu(CH_3)_2]^+$  complex in MeOH solution. Figure 3 shows a schematic representation of the energy barriers for the reductive elimination step for several model systems; all calculations include continuum solvent method. We employed analogous models to those considered in the previous section. This means including 0, 1 and 2 explicit MeOH on the calculations, which lead to complexes **1E-I**, **2E** and **2E-2**, respectively. Moreover, the gold complex including a solvation sphere of 5.5 Å around the metal center **2E-12** (with 12 explicit MeOH molecules) was also evaluated.

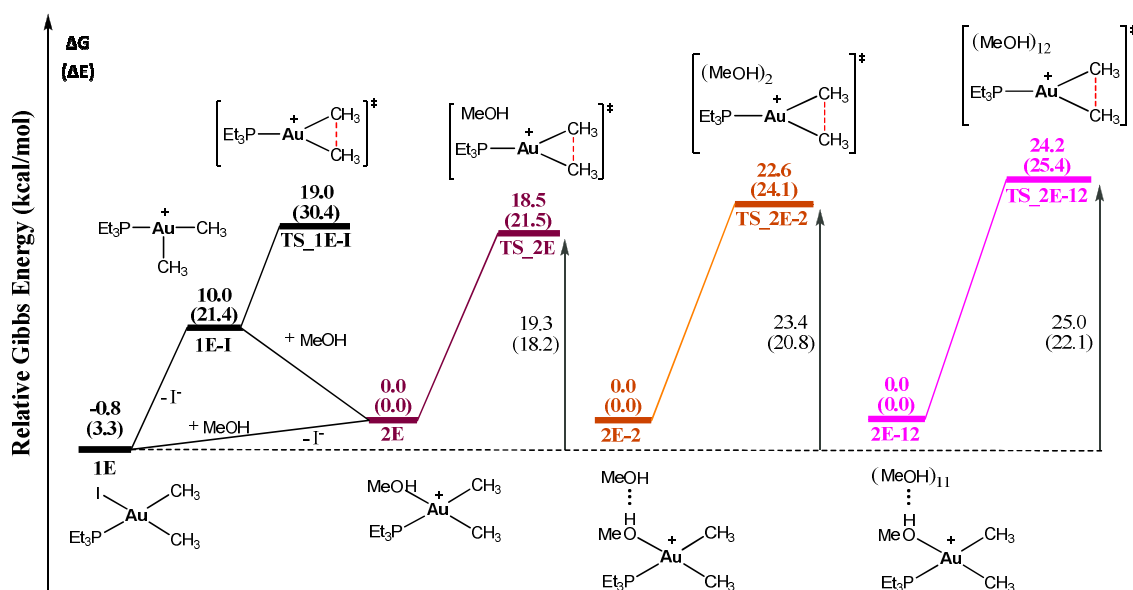


**Figure 3.** Gibbs energy barriers for the reductive elimination from species **1E**, **2E**, **2E-2** and **2E-12** in solution. Energies in kcal/mol; Potential energies in parenthesis.

The starting reactant, **1E**, is the most stable form in Gibbs energy in solution. According to the experimental proposal **1E** evolves to form a Au(III) cationic species. This intermediate can be either **1E-I**, a three-coordinated  $[(Et_3P)Au(CH_3)_2]^+$  species, or **2E**, a square-planar  $[(Et_3P)Au(MeOH)(CH_3)_2]^+$  species (Figure 3). These intermediates are schematically described by losing a iodide ligand. The Gibbs energy difference between **1E-I** and **2E** is 10.0 kcal/mol, the latter more stable.<sup>76</sup> This clearly shows that the

involved intermediate should include a solvent molecule (MeOH) occupying the “free” coordination site. This result reveals the difficulty of the continuum model to reproduce the explicit solvation in the coordination sphere of solute. The energy difference between reactant **1E** and intermediate **2E** is 0.8 kcal/mol, indicating that such intermediate is readily accessible. Moreover, the Gibbs energy barrier starting from **1E** and proceeding through **2E** intermediate is lower than that proceeding through **1E-I**. Overall, these results suggest that the initial cationic intermediate in solution is **2E**.

The reaction from complex **2E** has an overall Gibbs energy barrier for the reductive elimination of 19.3 kcal/mol. The geometry of the transition state, **TS\_2E**, shows that the MeOH is no longer directly bonded to the Au center with an Au...O<sub>MeOH</sub> distance of 3.320 Å. The forming C-C bond distance is 2.172 Å, Figure S14. The system with two explicit MeOH molecules, **2E-2**, increases the Gibbs energy barrier to 23.4 kcal/mol. At the transition state, **TS\_2E-2**, the MeOH is not coordinated to the gold center with a Au...O<sub>MeOH</sub> distance of 3.198 Å; the C-C bond forming distance is 2.150 Å, practically identical to the previous model. Given the barrier increase observed, we decided to evaluate a system including an explicit solvation sphere in addition to the continuum model.<sup>77</sup> The Gibbs energy barrier including 12 explicit MeOH, **TS\_2E-12**, is 25.0 kcal/mol. Notice that this value is in excellent agreement with experimental value observed for the reaction in solution,  $\Delta G^{\ddagger}_{\text{uncat,exp}} = 26.7$  kcal/mol.<sup>35</sup> Regarding the geometry of **TS\_2E-12** is very similar to previous cases with a forming C-C bond distance of 2.177 Å, and an Au...O<sub>MeOH</sub> distance of 3.419 Å (Figure S15). For the sake of completeness, the barrier for the system without any explicit MeOH molecule was also calculated. The three-coordinated species **1E-I** requires 10.8 kcal/mol to reach the transition state **TS\_1E-I**, whereas the overall barrier for the reductive elimination is 19.8 kcal/mol (Figure 3). For all computed systems the Gibbs energy barriers are higher than the analogous systems within metallocage.

For comparison, the reactions in vacuum were also calculated. The barrier from **1E-I** to **TS\_1E-I** is 3.3 kcal/mol, in agreement with the reported value of 1.7 kcal/mol for the reductive elimination calculated in a closely related process.<sup>53</sup> The barriers for systems **2E** and **2E-12** in vacuum are 18.6 and 20.0, respectively. In all cases the presence of a reaction field increases the reaction barrier. The continuum model, however, is not enough to properly describe the process and explicit molecules are required; adding explicit solvent molecules improve solvation calculations.<sup>63,78</sup> Looking at Figure 3 one can observe that the representation of the microenvironment plays a crucial role on the barrier of the process. The higher the number of explicit solvent molecules included in the model the higher the reductive elimination barrier. In other words, the more “naked” is the Au(III) complex, the lower is the reductive elimination barrier. Importantly, according to this, if the reaction can be performed in an environment where solvent molecules are removed the process is faster.

The dramatic energetic difference by modifying the microenvironment is not reflected on the geometries of the transition states; they show similar forming C-C bond

distances and the MeOH initially coordinated leaves the coordination sphere of the gold complex. The reaction is not well reproduced by a pure continuum model and a proper representation of the microenvironment is needed. The interactions between the gold complex and the microenvironment, inside the metallocage and in solution, are analyzed in the subsequent section.

### 3.4 Origin of catalysis by the presence of the $[\text{Ga}_4\text{L}_6]^{12-}$ metallocage

From the previous sections we learned that: (i) the model that better describes the process inside the metallocage is the one including one (coordinated) solvent molecule explicitly in the system, (ii) the calculated barrier for reduction elimination step decreases by removing explicit solvent molecules around the gold complex (both in solution and inside the metallocage), and (iii) the reductive elimination step is accelerated when it takes place inside the metallocage compared to the process in solution. With all these data in mind one can envisage the overall process divided in two formal processes. Starting from the complex in solution the first process consists in removing explicit solvent molecules around the gold complex (leaving only the MeOH coordinated to the metal center, as it is found within the cavity), and the second process is embedding the metal complex inside the metallocage. Figure 4 shows a schematic representation on how each of these two formal processes affects the reaction barrier.

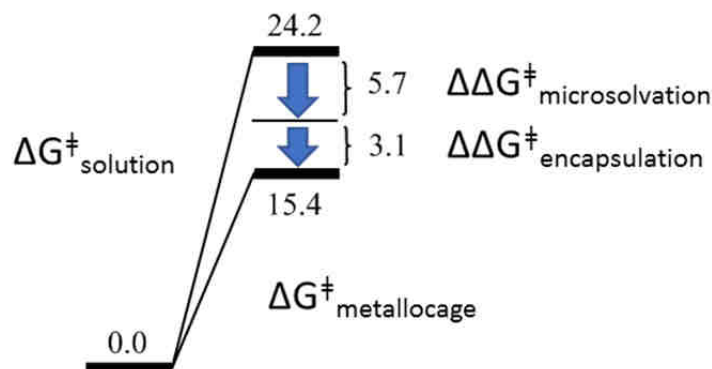


**Figure 4.** Decomposition of the decrease in the Gibbs energy barrier in two formal processes related to microsolvation and encapsulation. Gibbs energies in kcal/mol.

Considering the results from the two previous sections the energy associated to these two formal processes can be calculated. The effect on the Gibbs energy barrier by removing explicit solvent molecules is decreasing the barrier by 5.7 kcal/mol (from 25.0 kcal/mol in **TS\_2E-12** to 19.3 kcal/mol in **TS\_2E**, see Figure 3). Regarding the encapsulation process, comparing the Gibbs energy barrier for the reductive elimination in solution, (**2E** to **TS\_2E**,  $\Delta G^\ddagger=18.5$  kcal/mol), with that inside the metallocage, (**2E $\subset$ 3** to **TS\_2E $\subset$ 3**,  $\Delta G^\ddagger=15.4$  kcal/mol), this difference in the Gibbs energy is 3.1 kcal/mol; it can be associated to the reduction by performing the reaction inside the metallocage. Overall, the decrease in the Gibbs energy barrier by comparing the process in solution and inside the metallocage is 8.8 kcal/mol (5.7 kcal/mol for removing explicit microsolvation and 3.1 kcal/mol for encapsulation).

To investigate the origin of rate enhancement by the presence of the metallocage we performed an energy decomposition analysis similar to that employed by Himo et al. in their work with capsules.<sup>41</sup> It uses potential energies, nearly equivalent to enthalpies, instead of Gibbs energies (see section 7 and 8 of Sup. Inf.). Such analysis was very useful to identify strain and interaction energies associated to the encapsulation and microsolvation processes. The strain term does not significantly contribute to the process; thus, the modification of the geometry along the process (from reactant to transition state) is quite similar, not depending on the environment. The most important contribution to the barrier reduction clearly comes from the interaction energy, mainly associated to the encapsulation process. Such an interaction term can be mostly related to an electrostatic interaction (there are no covalent bonds between reactants and the cage).<sup>79</sup> This is completely consistent with previous experimental<sup>80</sup> and theoretical<sup>53</sup> results.

The Gibbs energies are calculated by adding the thermal corrections ( $\Delta Th$ ) to the potential energies ( $\Delta E_{\text{solv}}$ ); the former term is roughly associated to the entropic contributions. These magnitudes are schematically represented in Figure 5 for the process in solution (including 12 MeOH; pink profile), for the process including 1 MeOH solvent molecule (purple profile), and for the process inside metallocage **3** (green profile).

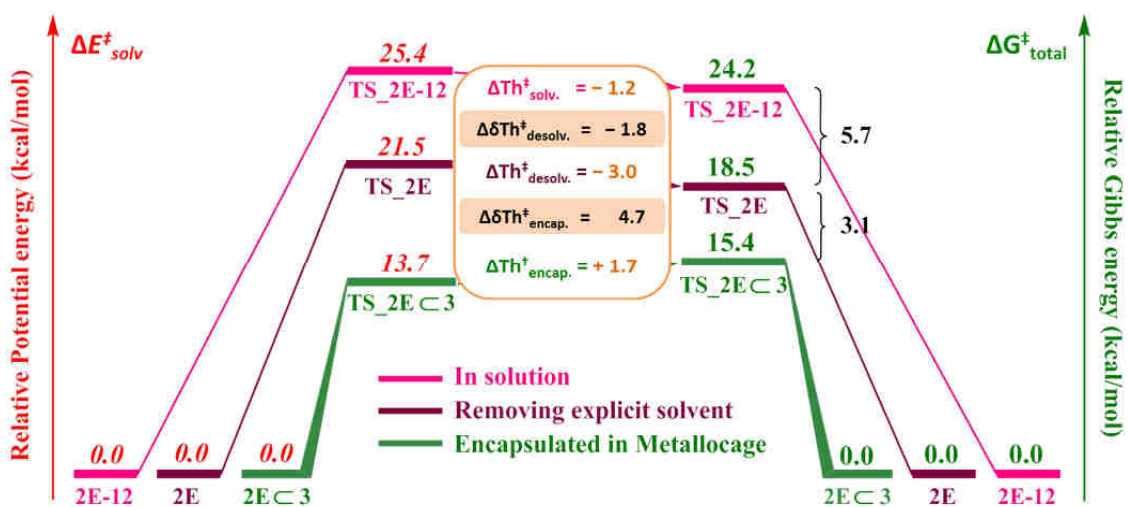


**Figure 5.** Schematic representation of the decomposition of Gibbs energy barriers (green numbers) in potential energy barriers (red numbers) and their respective thermal contributions (orange numbers). The analysis of model reaction of complex **2E** (purple profile), encapsulated complex (**2E<3**; green profile) and microsolvated complex (**2E-12**; pink profile) Energies in kcal/mol. Add 5.7 and 3.1

Regarding the entropic contributions to the overall process, the term related to remove the microsolvation,  $\Delta\delta Th_{\text{desolv}}^{\ddagger}$  diminish the barrier by -1.8 kcal/mol [ $-3.0 - (-1.2)$  kcal/mol], whereas the term related to the encapsulation process raises the barrier by 4.7 kcal/mol [ $+1.7 - (-3.0)$  kcal/mol]. Interestingly, the first term favors the reaction whereas the second is detrimental for the barrier. Overall, entropic contributions increase the barrier by 2.9 kcal/mol. The general view about

encapsulated chemical reactions is that entropy effects should favor the reaction because reactants are confined. Checking in literature recent computational works on supramolecular catalysis in most cases entropy was found to favor the process (in all these works the reaction was a bimolecular process).<sup>39–42,50</sup> In the reaction we are analyzing, however, the process is unimolecular generating two molecules starting from a single one, thus, the entropy may play an opposite role inside the metallocage.

In summary, the Gibbs energy barrier decrease was quantified as -5.7 and -3.1 kcal/mol, for each formal process, microsolvation and encapsulation, respectively. Encapsulating the complex reduces the barrier but removing explicit solvent molecules around the gold complex is even more significant for catalyzing the process. This suggests that for this C-C reductive elimination over a Au(III) complex, designing a cage (with similar electrostatic interactions) that fits better to the “naked” gold complex should improve the reaction rate. In this sense, one can envisage that designing a cage that favors the T-shaped complex should improve even more the reaction.

#### 4. CONCLUSIONS

The reductive elimination to form an alkyl-alkyl bond from a Au(III) complex in MeOH solution and inside a supramolecular  $[\text{Ga}_4\text{L}_6]^{12-}$  metallocage was investigated by means of computational methods to identify the factors that cause the rate acceleration of the reaction. Classical molecular dynamics simulations were performed to evaluate the behavior of the gold complex inside the cavity in combination with DFT calculations to analyze the reactivity.

Molecular dynamics calculations show that metallocage **3** accommodates the square planar complex  $[(\text{Et}_3\text{P})\text{Au}(\text{MeOH})(\text{CH}_3)_2]^+$ , **2E**, although an additional solvent molecule could also fit within the cavity. Moreover, simulation of T-shaped Au(III) complex,  $[(\text{Et}_3\text{P})\text{Au}(\text{CH}_3)_2]^+$  **1E-I**, along with a iodide ion inside the metallocage shows that iodide leaves the cavity very early, suggesting that the cationic Au(III) complex **2E** is the one encapsulated, in agreement with experimental proposal.

The DFT mechanistic analysis on the C-C reductive elimination reaction in both solvent and metallocage was also performed. According to the results the catalytic process can be divided in two formal processes. The first one can be described as removing explicit microsolvation of the  $[(\text{Et}_3\text{P})\text{Au}(\text{MeOH})(\text{CH}_3)_2]^+$  complex (keeping only one MeOH coordinated to the metal center, complex **2E**). The second process corresponds to the encapsulation inside the metallocage, **2E**  $\subset$  **3**. According to this, the overall 8.8 kcal/mol Gibbs energy barrier reduction by performing the reaction within metallocage **3**, can be divided in 5.7 kcal/mol for explicit desolvation and 3.1 kcal/mol for encapsulation, respectively. These results clearly suggest that the better the complex fits within the cavity (thus removing the surrounding solvent molecules) the larger the reduction in the energy barrier. This is a key point because recognizes the importance of the supramolecular cage on removing the solvent molecules around the Au(III) complex. On the other hand, encapsulation process itself is also important to reduce the Gibbs

energy barrier. The energy decomposition analysis shows that among the strain, interaction and thermal terms for the overall process the interaction energy is by far the most important one. We are working on other systems to see how these observations can be generalized. We believe that the identification of the contributions to the rate acceleration by the  $[\text{Ga}_4\text{L}_6]^{12-}$  metallocage might guide the design of new supramolecular catalysts.

## ASSOCIATED CONTENT

**Supporting Information.** Optimized geometries of model reactants and transition states that include counter ions, absolute energies and cartesian coordinates of all species, and analysis of the classical molecular dynamic simulation of host-guest complexes, parameters for molecular dynamics. "This material is available free of charge via the Internet at <http://pubs.acs.org>."

## AUTHOR INFORMATION

### Corresponding Author

\*Correspondence: Jean Didier Maréchal ([jeandidier.marechal@uab.cat](mailto:jeandidier.marechal@uab.cat)); Gregori Ujaque ([gregori.ujaque@uab.cat](mailto:gregori.ujaque@uab.cat))

### Author Contributions

The manuscript was written through contributions of all authors. All authors have given approval to the final version of the manuscript.

### Funding Sources

Projects n<sup>o</sup> CTQ-2017-87889-P, 2017SGR1323.

## ACKNOWLEDGMENT

The authors acknowledge the financial support of the Spanish MINECO-FEDER (Grants CTQ2017-87889-P and CTQ2016-81797-REDC). UAB is also acknowledged by a PIF grant to G.N., and Generalitat de Catalunya for grant 2017SGR1323.

## ABBREVIATIONS

DFT, density functional theory; B3LYP-D3, dispersion corrected Becke three parameter Lee-Yang-Parr exchange-correlation functional; SMD, solvent model density; PCM, polarizable continuum model, quasi-RRHO, quasi-rigid-rotor-harmonic-oscillator approximation, DLPNO-CCSD(T), domain based local pair-natural orbital coupled-cluster method, MD, molecular dynamics, MEOHBOX, methanol model, MCPB.py, python-based metal center parameter builder program, RESP, restrained electrostatic potential method.

## References

- (1) Ballester, P.; van Leeuwen, P. W. N. M.; Vidal-Ferran, A. *Supramolecular*

- Catalysis*, Reference Module in Chemistry, Molecular Sciences and Chemical Engineering, Elsevier, **2015**, 1-32.
- (2) Takeda, N.; Umemoto, K.; Yamaguchi, K.; Fujita, M. A Nanometre-Sized Hexahedral Coordination Capsule Assembled from 24 Components. *Nature*. **1999**, *398*, 794–796.
  - (3) Otte, M. Size-Selective Molecular Flasks. *ACS Catal.* **2016**, *6*, 6491–6510.
  - (4) Körner, S. K.; Tucci, F. C.; Rudkevich, D. M.; Heinz, T.; Rebek, J., Jr. A Self-Assembled Cylindrical Capsule: New Supramolecular Phenomena through Encapsulation. *Chem. - Eur. J.* **2002**, *6*, 187–195.
  - (5) Kang, J.; Rebek, J., Jr. Acceleration of a Diels-Alder Reaction by a Self-assembled Molecular Capsule. *Nature*. **1997**, *385*, 50–52.
  - (6) Kang, J.; Santamaria, J.; Hilmersson, G.; Rebek J., Jr. Self-Assembled Molecular Capsule Catalyzes a Diels-Alder Reaction. *J. Am. Chem. Soc.* **1998**, *120*, 7389–7390.
  - (7) Stang, P. J.; Olenyuk, B. Self-Assembly, Symmetry, and Molecular Architecture: Coordination as the Motif in the Rational Design of Supramolecular Metallacyclic Polygons and Polyhedra. *Acc. Chem. Res.* **1997**, *30*, 502-518.
  - (8) Caulder, D. L.; Powers, R. E.; Parac, T. N.; Raymond, K. N. The Self-Assembly of a Predesigned Tetrahedral  $M_4L_6$  Supramolecular Cluster. *Angew. Chem., Int. Ed.* **1998**, *37*, 1840–1843.
  - (9) Pluth, M. D.; Bergman, R. G.; Raymond, K. N. Proton-Mediated Chemistry and Catalysis in a Self-Assembled Supramolecular Host. *Acc. Chem. Res.* **2009**, *42*, 1650–1659.
  - (10) Petrosko, S. H.; Johnson, R.; White, H.; Mirkin, C. A. Nanoreactors: Small Spaces, Big Implications in Chemistry. *J. Am. Chem. Soc.* **2016**, *138*, 7443–7445.
  - (11) Ward, M. D.; Hunter, C. A.; Williams, N. H. Coordination Cages Based on Bis(Pyrazolylpyridine) Ligands: Structures, Dynamic Behavior, Guest Binding, and Catalysis. *Acc. Chem. Res.* **2018**, *51*, 2073–2082.
  - (12) Datta, S.; Saha, M. L.; Stang, P. J. Hierarchical Assemblies of Supramolecular Coordination Complexes. *Acc. Chem. Res.* **2018**, *51*, 2047–2063.
  - (13) Zhang, D.; Ronson, T. K.; Nitschke, J. R. Functional Capsules via Subcomponent Self-Assembly. *Acc. Chem. Res.* **2018**, *51*, 2423–2436.
  - (14) Jongkind, L. J.; Caumes, X.; Hartendorp, A. P. T.; Reek, J. N. H. Ligand Template Strategies for Catalyst Encapsulation. *Acc. Chem. Res.* **2018**, *51*, 2115–2128.
  - (15) Zhang, Q.; Catti, L.; Tiefenbacher, K. Catalysis inside the Hexameric Resorcinarene Capsule. *Acc. Chem. Res.* **2018**, *51*, 2107–2114.
  - (16) Pullen, S.; Clever, G. H. Mixed-Ligand Metal-Organic Frameworks and Heteroleptic Coordination Cages as Multifunctional Scaffolds - A Comparison.



*Acc. Chem. Res.* **2018**, *51*, 3052–3064.

- (17) Vriezema, D. M.; Comellas Aragonès, M.; Elemans, J. A. A. W.; Cornelissen, J. J. L. M.; Rowan, A. E.; Nolte, R. J. M. Self-Assembled Nanoreactors. *Chem. Rev.* **2005**, *105*, 1445–1490.
- (18) Koblenz, T. S.; Wassenaar, J.; Reek, J. N. H. Reactivity within a Confined Self-Assembled Nanospace. *Chem. Soc. Rev.* **2008**, *37*, 247–262.
- (19) Raynal, M.; Ballester, P.; Vidal-Ferran, A.; van Leeuwen, P. W. N. M. Supramolecular Catalysis. Part 2: Artificial Enzyme Mimics. *Chem. Soc. Rev.* **2014**, *43*, 1734–1787.
- (20) Leenders, S. H. A. M.; Gramage-Doria, R.; de Bruin, B.; Reek, J. N. H. Transition Metal Catalysis in Confined Spaces. *Chem. Soc. Rev.* **2015**, *44*, 433–448.
- (21) Vardhan, H.; Verpoort, F. Metal-Organic Polyhedra: Catalysis and Reactive Intermediates. *Adv. Synth. Catal.* **2015**, *357*, 1351–1368.
- (22) Caulder, D. L.; Brückner, C.; Powers, R. E.; König, S.; Parac, T. N.; Leary, J. A.; Raymond, K. N. Design, Formation and Properties of Tetrahedral M<sub>4</sub>L<sub>4</sub> and M<sub>4</sub>L<sub>6</sub> Supramolecular Clusters. *J. Am. Chem. Soc.* **2001**, *123*, 8923–8938.
- (23) Yoshizawa, M.; Tamura, M.; Fujita, M. Diels-Alder in Aqueous Molecular Hosts: Unusual Regioselectivity and Efficient Catalysis. *Science*. **2006**, *312*, 251–254.
- (24) Bolliger, J. L.; Belenguer, A. M.; Nitschke, J. R. Enantiopure Water-Soluble [Fe<sub>4</sub>L<sub>6</sub>] Cages: Host-Guest Chemistry and Catalytic Activity. *Angew. Chem., Int. Ed.* **2013**, *52*, 7958–7962.
- (25) Amouri, H.; Desmarets, C.; Moussa, J. Confined Nanospaces in Metallocages: Guest Molecules, Weakly Encapsulated Anions, and Catalyst Sequestration. *Chem. Rev.* **2012**, *112*, 2015–2041.
- (26) Brown, C. J.; Toste, F. D.; Bergman, R. G.; Raymond, K. N. Supramolecular Catalysis in Metal–Ligand Cluster Hosts. *Chem. Rev.* **2015**, *115*, 3012–3035.
- (27) García-Simón, C.; Gramage-Doria, R.; Raoufmoghaddam, S.; Parella, T.; Costas, M.; Ribas, X.; Reek, J. N. H. Enantioselective Hydroformylation by a Rh-Catalyst Entrapped in a Supramolecular Metallocage. *J. Am. Chem. Soc.* **2015**, *137*, 2680–2687.
- (28) Pluth, M. D.; Bergman, R. G.; Raymond, K. N. Acid Catalysis in Basic Solution: a supramolecular host promotes orthoformate hydrolysis. *Science*. **2007**, *316*, 85–88.
- (29) Hastings, C. J.; Pluth, M. D.; Bergman, R. G.; Raymond, K. N. Enzymelike Catalysis of the Nazarov Cyclization by Supramolecular Encapsulation. *J. Am. Chem. Soc.* **2010**, *132*, 6938–6940.
- (30) Wang, Z. J.; Brown, C. J.; Bergman, R. G.; Raymond, K. N.; Toste, F. D. Hydroalkoxylation Catalyzed by a Gold(I) Complex Encapsulated in a Supramolecular Host. *J. Am. Chem. Soc.* **2011**, *133*, 7358–7360.

- (31) Leung, D. H.; Bergman, R. G.; Raymond, K. N. Highly Selective Supramolecular Catalyzed Allylic Alcohol Isomerization. *J. Am. Chem. Soc.* **2007**, *129*, 2746–2747.
- (32) Brown, C. J.; Bergman, R. G.; Raymond, K. N. Enantioselective Catalysis of the Aza-Cope Rearrangement by a Chiral Supramolecular Assembly. *J. Am. Chem. Soc.* **2009**, *131*, 17530–17531.
- (33) Leung, D. H.; Bergman, R. G.; Raymond, K. N. Scope and Mechanism of the C-H Bond Activation Reactivity within a Supramolecular Host by an Iridium Guest: A Stepwise Ion Pair Guest Dissociation Mechanism. *J. Am. Chem. Soc.* **2006**, *128*, 9781–9797.
- (34) Hong, C. M.; Bergman, R. G.; Raymond, K. N.; Toste, F. D. Self-Assembled Tetrahedral Hosts as Supramolecular Catalysts. *Acc. Chem. Res.* **2018**, *51*, 2447–2455.
- (35) Kaphan, D. M.; Levin, M. D.; Bergman, R. G.; Raymond, K. N.; Toste, F. D. A Supramolecular Microenvironment Strategy for Transition Metal Catalysis. *Science*. **2015**, *350*, 1235–1238.
- (36) Levin, M. D.; Kaphan, D. M.; Hong, C. M.; Bergman, R. G.; Raymond, K. N.; Toste, F. D. Scope and Mechanism of Cooperativity at the Intersection of Organometallic and Supramolecular Catalysis. *J. Am. Chem. Soc.* **2016**, *138*, 9682–9693.
- (37) Houk, K. N. Foreword: Applied Computational Chemistry. *Chem. Soc. Rev.* **2014**, *43*, 4905–4905.
- (38) Tantillo, D. J. Faster, Catalyst! React! React! Exploiting Computational Chemistry for Catalyst Development and Design. *Acc. Chem. Res.* **2016**, *49*, 1079–1079.
- (39) Goehry, C.; Besora, M.; Maseras, F. Computational Study on the Mechanism of the Acceleration of 1,3-Dipolar Cycloaddition inside Cucurbit[6]Uril. *ACS Catal.* **2015**, *5*, 2445–2451.
- (40) Carlqvist, P.; Maseras, F. A Theoretical Analysis of a Classic Example of Supramolecular Catalysis. *Chem. Commun.* **2007**, 748–750.
- (41) Daver, H.; Harvey, J. N.; Rebek, J., Jr.; Himo, F. Quantum Chemical Modeling of Cycloaddition Reaction in a Self-Assembled Capsule. *J. Am. Chem. Soc.* **2017**, *139*, 15494–15503.
- (42) Kim, S. P.; Leach, A. G.; Houk, K. N. The Origins of Noncovalent Catalysis of Intermolecular Diels-Alder Reactions by Cyclodextrins, Self-Assembling Capsules, Antibodies, and RNAses. *J. Org. Chem.* **2002**, *67*, 4250–4260.
- (43) Xu, L.; Hua, W.; Hua, S.; Li, J.; Li, S. Mechanistic Insight on the Diels-Alder Reaction Catalyzed by a Self-Assembled Molecular Capsule. *J. Org. Chem.* **2013**, *78*, 3577–3582.
- (44) Karnes, J. J.; Benjamin, I. S<sub>N</sub>2 Reaction Rate Enhancement by  $\beta$ -Cyclodextrin at the Liquid/Liquid Interface. *J. Phys. Chem. C* **2017**, *121*, 19209–19217.
- (45) Furuki, T.; Hosokawa, F.; Sakurai, M.; Inoue, Y.; Chujo, R. Microscopic Medium

- Effects on a Chemical Reaction. A Theoretical Study of Decarboxylation Catalyzed by Cyclodextrins as an Enzyme Model. *J. Am. Chem. Soc.* **1993**, *115*, 2903–2911.
- (46) Sarmentero, M. A.; Fernández-Pérez, H.; Zuidema, E.; Bo, C.; Vidal-Ferran, A.; Ballester, P. Catalytic Hydrogenation of Norbornadiene by a Rhodium Complex in a Self-Folding Cavitand. *Angew. Chem., Int. Ed.* **2010**, *49*, 7489–7492.
- (47) Ruiz-Botella, S.; Vidossich, P.; Ujaque, G.; Peris, E. Rim, Side Arms, and Cavity: Three Sites for the Recognition of Anions by Tetraazolium Resorcinarene Cavitands. *Chem. - Eur. J.* **2016**, *22*, 15800–15806.
- (48) Daver, H.; Algarra, A. G.; Rebek, J., Jr.; Harvey, J. N.; Himo, F. Mixed Explicit-Implicit Solvation Approach for Modeling of Alkane Complexation in Water-Soluble Self-Assembled Capsules. *J. Am. Chem. Soc.* **2018**, *140*, 12527–12537.
- (49) Turcani, L.; Berardo, E.; Jelfs, K. E. Stk: A Python Toolkit for Supramolecular Assembly. *J. Comput. Chem.* **2018**, *39*, 1931–1942.
- (50) Goehry, C.; Besora, M.; Maseras, F. Computational Description of a Huisgen Cycloaddition Inside a Self-Assembled Nanocapsule. *Eur. J. Org. Chem.* **2018**, 2103–2109.
- (51) Frushicheva, M. P.; Mukherjee, S.; Warshel, A. Electrostatic Origin of the Catalytic Effect of a Supramolecular Host Catalyst. *J. Phys. Chem. B* **2012**, *116*, 13353–13360.
- (52) Ootani, Y.; Akinaga, Y.; Nakajima, T. Theoretical Investigation of Enantioselectivity of Cage-like Supramolecular Assembly: The Insights into the Shape Complementarity and Host-Guest Interaction. *J. Comput. Chem.* **2015**, *36*, 459–466.
- (53) Vaissier-Welborn, V.; Head-Gordon, T. Electrostatics Generated by a Supramolecular Capsule Stabilizes the Transition State for Carbon-Carbon Reductive Elimination from Gold(III) Complex. *J. Phys. Chem. Lett.* **2018**, *9*, 3814–3818.
- (54) Becke, A. D. Density-Functional Thermochemistry. III. The Role of Exact Exchange. *J. Chem. Phys.* **1993**, *98*, 5648–5652.
- (55) Gaussian 09, Revision D.01, M. J. Frisch, G. W. Trucks, H. B. Schlegel, G. E. Scuseria, M. A. Robb, J. R. Cheeseman, G. Scalmani, V. Barone, B. Mennucci, G. A. Petersson, H. Nakatsuji, M. Caricato, X. Li, H. P. Hratchian, A. F. Izmaylov, J. Bloino, G. Zheng, J. L. Sonnenberg, M. Hada, M. Ehara, K. Toyota, R. Fukuda, J. Hasegawa, M. Ishida, T. Nakajima, Y. Honda, O. Kitao, H. Nakai, T. Vreven, J. A. Montgomery, Jr., J. E. Peralta, F. Ogliaro, M. Bearpark, J. J. Heyd, E. Brothers, K. N. Kudin, V. N. Staroverov, T. Keith, R. Kobayashi, J. Normand, K. Raghavachari, A. Rendell, J. C. Burant, S. S. Iyengar, J. Tomasi, M. Cossi, N. Rega, J. M. Millam, M. Klene, J. E. Knox, J. B. Cross, V. Bakken, C. Adamo, J. Jaramillo, R. Gomperts, R. E. Stratmann, O. Yazyev, A. J. Austin, R. Cammi, C. Pomelli, J. W. Ochterski, R. L. Martin, K. Morokuma, V. G. Zakrzewski, G. A. Voth, P. Salvador, J. J. Dannenberg, S. Dapprich, A. D. Daniels, O. Farkas, J. B. Foresman, J. V. Ortiz, J.

Cioslowski, D. J. Fox, Gaussian, Inc., Wallingford CT, **2013**.

- (56) Höllwarth, A.; Böhme, M.; Dapprich, S.; Ehlers, A. W.; Gobbi, A.; Jonas, V.; Köhler, K. F.; Stegmann, R.; Veldkamp, A.; Frenking, G. A Set of d-Polarization Functions for Pseudo-Potential Basis Sets of the Main Group Elements Al-Bi and f-Type Polarization Functions for Zn, Cd, Hg. *Chem. Phys. Lett.* **1993**, *208*, 237–240.
- (57) Ehlers, A. W.; Böhme, M.; Dapprich, S.; Gobbi, A.; Höllwarth, A.; Jonas, V.; Köhler, K. F.; Stegmann, R.; Veldkamp, A.; Frenking, G. A Set of f-Polarization Functions for Pseudo-Potential Basis Sets of the Transition Metals Sc-Cu, Y-Ag and La-Au. *Chem. Phys. Lett.* **1993**, *208*, 111–114.
- (58) Marenich, A. V.; Cramer, C. J.; Truhlar, D. G. Universal Solvation Model Based on Solute Electron Density and on a Continuum Model of the Solvent Defined by the Bulk Dielectric Constant and Atomic Surface Tensions. *J. Phys. Chem. B* **2009**, *113*, 6378–6396.
- (59) Grimme, S.; Antony, J.; Ehrlich, S.; Krieg, H. A Consistent and Accurate ab initio Parametrization of Density Functional Dispersion Correction (DFT-D) for the 94 Elements H-Pu. *J. Chem. Phys.* **2010**, *132*, 154104–154119.
- (60) Miertuš, S.; Scrocco, E.; Tomasi, J. Electrostatic Interaction of a Solute with a Continuum. A Direct Utilization of ab initio Molecular Potentials for the Prevision of Solvent Effects. *Chem. Phys.* **1981**, *55*, 117-129.
- (61) Tomasi, J.; Mennucci, B.; Cammi, R. Quantum mechanical continuum solvation models. *Chem. Rev.* **2005**, *105*, 2999-3093.
- (62) Grimme, S. Supramolecular Binding Thermodynamics by Dispersion-Corrected Density Functional Theory. *Chem. - Eur. J.* **2012**, *18*, 9955–9964.
- (63) Bryantsev, V. S.; Diallo, M. S.; Goddard, W. A. Calculation of Solvation Free Energies of Charged Solutes Using Mixed Cluster/Continuum Models. *J. Phys. Chem. B* **2008**, *112*, 9709–9719.
- (64) Paulechka, E.; Kazakov, A. Efficient DLPNO-CCSD(T)-Based Estimation of Formation Enthalpies for C-, H-, O-, and N-Containing Closed-Shell Compounds Validated Against Critically Evaluated Experimental Data. *J. Phys. Chem. A* **2017**, *121*, 4379–4387.
- (65) Neese, F. Software Update: The ORCA Program System, Version 4.0. *WIREs Comput. Mol. Sci.* **2018**, *8*, e1327.
- (66) D. A. Case, R.M. Betz, D.S. Cerutti, T.E. Cheatham, III, T.A. Darden, R.E. Duke, T.J. Giese, H. Gohlke, A.W. Goetz, N. Homeyer, S. Izadi, P. Janowski, J. Kaus, A. Kovalenko, T.S. Lee, S. LeGrand, P. Li, C. Lin, T. Luchko, R. Luo, B. Madej, D. Mermelstein, K.M. Merz, G. Monard, H. Nguyen, H.T. Nguyen, I. Omelyan, A. Onufriev, D.R. Roe, A. Roitberg, C. Sagui, C.L. Simmerling, W.M. Botello-Smith, J. Swails, R.C. Walker, J. Wang, R.M. Wolf, X. Wu, L. Xiao and P.A. Kollman (2016), *AMBER 2016*, University of California, San Francisco.
- (67) Wang, J.; Wolf, R. M.; Caldwell, J. W.; Kollman, P. A.; Case, D. A. Development

- and Testing of a General Amber Force Field. *J. Comput. Chem.* **2004**, *25*, 1157–1174.
- (68) Li, P.; Merz, K. M. MCPB.Py: A Python Based Metal Center Parameter Builder. *J. Chem. Inf. Model.* **2016**, *56*, 599–604.
- (69) Wang, J.; Wang, W.; Kollman, P. A.; Case, D. A. Automatic Atom Type and Bond Type Perception in Molecular Mechanical Calculations. *J. Mol. Graph. Model.* **2006**, *25*, 247–260.
- (70) Bayly, C. I.; Cieplak, P.; Cornell, W. D.; Kollman, P. A. A Well-Behaved Electrostatic Potential Based Method Using Charge Restraints for Deriving Atomic Charges: The RESP Model. *J. Phys. Chem.* **1993**, *97*, 10269–10280.
- (71) Kozlikova, B.; Sebestova, E.; Sustr, V.; Brezovsky, J.; Strnad, O.; Daniel, L.; Bednar, D.; Pavelka, A.; Manak, M.; Bezdeka, M.; Benes, P.; Kotry, M.; Gora, A.; Damborsky, J.; Sochor, J. CAVER Analyst 1.0: Graphic Tool for Interactive Visualization and Analysis of Tunnels and Channels in Protein Structures. *Bioinformatics.* **2014**, *30*, 2684–2685.
- (72) Andersen, U. N.; Seeber, G.; Fiedler, D.; Raymond, K. N.; Lin, D.; Harris, D. Characterization of self-assembled supramolecular [Ga<sub>4</sub>L<sub>6</sub>] host-guest complexes by electrospray ionization mass spectrometry. *J. Am. Soc. Mass. Spectrom.* **2006**, *17*, 292–296.
- (73) Another configuration of the **TS\_2E@3** is found to be 1.3 kcal/mol higher in Gibbs energy than the one included in the main text; (See SI).
- (74) A non-covalent interaction (NCI) analysis between the substrate and the metallocage at **2E** and **TS\_2E<3** shows that at the transition state there is a H-bond between the leaving MeOH and an oxygen from the cage (missing in the reactant), and the interaction between the forming H<sub>3</sub>C···CH<sub>3</sub> and the naphthalene of the cage is stronger than in the reactant (see Figures S21 and S22); reference for NCI method: Johnson, E. R.; Keinan, S.; Mori-Sanchez, P.; Contreras-Garcia, J.; Cohen, A. J.; Yang, W. Revealing noncovalent interactions *J. Am. Chem. Soc.* **2010**, *132*, 6498-6506.
- (75) The number of K<sup>+</sup> counterions do not modify the barrier but highly affects binding energies. Binding energies of **2E** to **3** is -54.2 and to **3K11** is -32.1 kcal/mol, respectively.
- (76) The occupation of the “Free” binding site even in a non-coordinating solvent for a related Pd complex was shown by hybrid QM/MD calculations. See: Vidossich, P.; Ujaque, G.; Lledós, A. *Chem. Commun.* **2014**, *50*, 661–663.
- (77) From the molecular dynamics simulation of the **2E** complex in explicit MeOH solvent we took the last snapshot after 10 ns simulation to represent the microenvironment around this complex. Then, we explicitly included in the DFT calculation all the MeOH molecules contained within a radius of 5.5 Å from the Au center, for a total of 12 MeOH molecules.
- (78) Kelly, C. P.; Cramer, C. J.; Truhlar, D. G. Adding Explicit Solvent Molecules to

Continuum Solvent Calculations for the Calculation of Aqueous Acid Dissociation Constants. *J. Phys. Chem. A* **2006**, *110*, 2493–2499.

- (79) Zhang, X.; Houk, K. N. Why Enzymes Are Proficient Catalysts: Beyond the Pauling Paradigm. *Acc. Chem. Res.* **2005**, *38*, 379–385.
- (80) Hong, C. M.; Morimoto, M.; Kapustin, E. A.; Alzakhem, N.; Bergman, R. G.; Raymond, K. N.; Toste, F. D. Deconvoluting the Role of Charge in a Supramolecular Catalyst. *J. Am. Chem. Soc.* **2018**, *140*, 6591–6595.

## TOC Graphic

